The Cusp as a VLF Saucer Source: First Rocket Observations of Long-Duration VLF Saucers on the Dayside

C. Moser[1], J. LaBelle [1], S. Hatch[2], J.I. Moen[3,4], A. Spicher[3], T. Takahashi[3], C.A. Kletzing[5], S. Bounds[5], K. Oksavik[2,4], F. Sigernes[4], T.K. Yeoman[6]

to be submitted to Geophysical Research Letters

[1]Department of Physics and Astronomy, Dartmouth College, Hanover
[2]Birkeland Centre for Space Science, Department of Physics and Technology, University of Bergen, Norway
[3]Department of Physics, University of Oslo, Oslo, Norway
[4]Department of Arctic Geophysics, University Centre in Svalbard, Longyearbyen, Norway
[5]Department of Physics and Astronomy, University of Iowa, Iowa City
[6]University of Leicester School of Physics and Astronomy, Leicester

Key Points:

- First observation of large-scale dayside saucers from a sounding rocket
- The saucer source regions are co-located with the polar cusp
- Alfvénically accelerated dispersed electrons observed in the cusp correspond to approximately the same source region as the saucer signals.

Plain Language:

Electrons precipitating down Earth's high-latitude magnetic field lines, which cause aurora at lower altitudes, emit radio waves at particular angles to the background magnetic field, depending on their frequency. When spacecrafts traverse through a region close to the source, they observe descending and ascending frequency signatures in their spectrograms referred to as saucers. Our research focused on the first rocket observations, from the CAPER-2 mission, of large scale, multi-armed saucers on the dayside as opposed to the nightside where they are most commonly observed. These observations are similar to those made recently with the DEMETER satellite, but include in-situ particle and conjugate ground-based measurements. Using ray-tracing software and hodogram analysis of the electric field waveforms combined with ground based radar measurements, we were able to determine the source location of the saucers to be in the cusp of earths magnetic field at altitudes near 2500 km. Additionally, particle measurements on board the rocket showed time dispersed bursts of electrons typically associated with Alfvénic acceleration, which can be traced back to a source height that is approximately equal to the source height of the observed saucers, suggesting the source of the radio waves is associated with the dispersed electrons.

Abstract

Auroral whistler mode radio emissions called saucers are of fundamental interest because they require an unusually stationary emission process in the dynamic auroral environment, and it is a mystery how that can happen in this or similar conditions elsewhere in geospace. The Cusp Alfvén and Plasma Electrodynamics Rocket (CAPER-2), launched into the polar cusp, obtained the first rocket measurements of a large-scale, multiple-armed dayside saucer, similar to those recently observed the the DEMETER satellite, with the addition of in situ particle measurements and simultaneous conjugate ground-based measurements. For 300 s prior to cusp entry, CAPER-2 detected ∼15 truncated saucer arms lasting 5–50 s. Directional analysis using waveforms, combined with ground-based data, suggests that these originate within the cusp. Ray-tracing analysis indicates source altitudes ∼2500 km. On-board particle instruments show dispersed electron bursts in the cusp, presumed Alfvénically accelerated, corresponding to approximately the same source heights as the saucers.

1 Introduction

VLF Auroral hiss is one of the most prevalent auroral radio emissions, detected by suitably instrumented spacecraft on almost every pass through aurora [reviews by Sazhin et al., 1993; LaBelle and Treumann, 2002]. Satellites often observe structured hiss such as VLF saucers which produce multiple nested V-shaped patterns in frequency-time spectrograms. Saucers are one of the earliest VLF phenomena reported from spacecraft, due to their distinctive appearance on spectrograms [Gurnett, 1966; Smith, 1969; Mosier and Gurnett, 1969]. Saucers are of broad interest because they demonstrate a wave phenomenon that is usually stationary despite the dynamic environment of the aurora. Original observations of saucers occurred in nightside low-Earth orbit auroral traversals, where downward going "funnel shaped" emissions were observed punctuated by upward-propagating saucers having durations of tens of seconds [e.g. Gurnett and Frank, 1972, Plates 4–5]. Saucers arise from propagation effects, whereby whistler mode signals of different frequencies generated on the "resonance cone" propagate at different angles relative to the background magnetic field; a satellite or rocket flying over or under the source sees a V-pattern of frequencies versus time. James [1976] showed how, assuming a point source, the saucer shapes and frequencies allow the distance from satellite to source to be inferred. Temerin [1979] generalized this analysis to include line sources. Lönnquist et al. [1993] showed that saucers occur at high altitudes up to 13000 km. Horita et al. [1982] showed that saucers can come from sources above the satellite as well as below. Ergun et al. [2001] showed dramatic multiple-armed saucers detected by the FAST satellite, with bursty electric fields at the vortices indicative of upward propagating phase space electron holes, implicating these features in the chain of causation. Kasahara et al. [1995] measure wave normal angles with the Akebono satellite confirming saucer signal generation on a resonance cone.

While most observations above concentrated on nightside aurora, it was known from an early date that saucers also occur on the dayside. For example, Yoshino et al. [1981] showed observations of VLF saucers on the dayside as well as nightside, finding a seasonal variation in source altitudes. James et al. [2012] made significant advances on the basis of dramatic multiple-armed saucers observed on the dayside with the DEMETER satellite. These dayside saucers lasted considerably longer than typical previously observed nightside examples, with durations up to 100 s, corresponding to up to 1000 km given spacecraft horizontal velocities (top left example in Figure 1 of James et al., [2012]). The source locations of these saucers were correspondingly inferred to be at great distances above the satellite, of order 3000 km. James et al. [2012] showed several examples suggesting that large-scale saucers with high altitude sources may be a regular feature of the dayside.

The recent CAPER-2 mission encountered a large scale saucer event similar to those reported by James et al. [2012], for the first time from a sounding rocket. Rocket observations including low energy field-aligned electron spectra and electric field waveforms, combined with ground-based imager data, suggest a connection between this event and the cusp.

2 Data Presentation

The CAPER-2 sounding rocket launched from Andøya, Norway, at 0927 UT on January 4, 2019, reaching an apogee of 774 km. The interplanetary magnetic field (IMF) was relatively stable, with IMF $B_z \approx -5$ nT and IMF $B_y \approx 2$–6 nT, for one to two hours prior to launch. Under these conditions, radar backscatter typical of cusp appeared over Svalbard measured with the Super Dual Auroral Radar Network (SuperDARN) [Chisham et al., 2007] at Hankasalmi, cusp signatures such as enhanced ionospheric density and temperature were measured by the EISCAT Svalbard radar using the upward-directed 42 m antenna, and red-line dominated cusp aurora was observed over Svalbard with ground-based imagers.

The CAPER-2 payload included field and electron instruments. The DC electric field perpendicular to the rocket spin axis, maintained within ten degrees of the background magnetic field direction, was measured with two radial double-probe antennas using 6-cm diameter probes with 3 m separation. The same radial booms/probes system was used to measure ELF (0–1 kHz) and VLF (1–40 kHz) electric fields. High frequency (HF) electric fields up to 5.0 MHz were measured with a radial double-probe antenna. CAPER-2 included two types of electron detectors: "bagel"-style detectors measured down-going electrons in eight selected energy ranges between 220 and 625 eV, and "top-hat" style detectors measured 0.2–12.3 keV electron distribution functions; however the top-hat returned limited data due to a software problem. The bagels, along with the HF receiver, comprised a wave-particle correlator instrument. CAPER-2 also included a flux-gate magnetometer and four needle Langmuir probes measuring electron density fluctuations at 8 kHz sample rate.

Figure 1 shows survey plots of selected data from the cusp crossing. Figure 1a is a 0–2.5 MHz electric field spectrogram. For most of the flight after 200 s the electron gyrofrequency (f_{ce}) exceeds the plasma frequency (f_{pe}); the latter appears as an upper cutoff of whistler-mode noise, descending from 1200 kHz at 210 s (408 km) on the up-leg to 300 kHz near apogee at 529 s (774 km, green circle). CAPER-2 enters the cusp at 490 s (769 km, red triangle), marked by the onset of low-energy downgoing electrons in Figure 1d. These electrons persist until approximately 700 s (670 km, red square) on the down-leg. During the 210 s interval in which CAPER-2 is within the cusp, intense Langmuir waves near f_{pe} appear in the HF spectrogram, and before and after this time intense whistler mode waves occur below f_{pe}. The plasma frequency increases above its ambient level during the cusp traversal, as expected from a combination of electron impact ionization and Joule heating enhancing the scale height. The second panel is a 0–40 kHz VLF electric field spectrogram, showing a band of whistler mode waves through much of the flight with lower cutoff near the lower hybrid frequency (f_{LH} ∼5 kHz). Broadband ELF waves occur below f_{LH} during the cusp traversal. Structured whistler mode emissions at 5–20 kHz appear at 200 s (385 km), several hundred seconds before the cusp encounter. Whistler mode waves in this frequency range continue during the cusp traversal but are less structured.

Figure 2 shows expanded views of the VLF spectrogram, covering 0–25 kHz and 180–450 s. Most striking are bursts of VLF waves marked by sharp lower cutoffs that descend in frequency with time. The bottom panel highlights twelve selected wave cutoffs seen in the top panel. These features resemble "VLF saucers," nested cone-like features at VLF frequencies, commonly observed with spacecraft traversing the auroral region [e.g., James, 1976; Ergun et al., 2001], and attributed to dispersion effects arising from waves generated on the whistler-mode resonance cone at a localized source above or below the spacecraft [James, 1976]. However, whereas saucers typically last a few seconds in the spacecraft frame, corresponding to tens of kilometers, the wave structures encountered by CAPER-2 persist for hundreds of kilometers prior to encountering the cusp, similar to dayside saucers observed with the DEMETER spacecraft [James et al. 2012]. The saucer-like waves observed by CAPER-2 are also asymmetric, occurring only on the equatorward side of the cusp.

Figure 2c, adapted from James [1976], illustrates the mechanism responsible for VLF saucers. The whistler mode is characterized by a resonance cone, a surface in k-space for which the index of refraction becomes large. On this resonance cone, the wave-normal direction is perpendicular to the group velocity direction. Hence, for waves on the resonance cone at the low-frequency end of the whistler range, near f_{LH}, the wave-normal direction is nearly perpendicular to the background B-field, and the ray direction is nearly parallel. For waves at the top end of the whistler range and near the lesser of f_{pe} or f_{ce}, the wave-normal is nearly parallel and the ray direction nearly perpendicular. Since the auroral electrons are relatively slow (energies $\leq$ 10 keV), they interact with whistler waves of high index of refraction on the resonance cone. A spacecraft passing under this source observes descending whistler mode frequencies until it reaches its closest approach to the source, after which it observes ascending frequencies.

The geometry of Figure 2c and magneto-ionic theory, assuming straight line propagation following James [1976], implies an expression for the saucer cutoff frequency as a function of source height, h:

$$f^2 = \frac{1}{2}\left(f_{uh}^2 \pm \sqrt{f_{uh}^4 - 4\frac{f_{ce}^2 f_{pe}^2 a^2}{(1+a^2)}}\right) \tag{1}$$

where $a = (x_0^2+v_s^2(t-t_0)^2/h$ and $f_{uh}^2 = f_{pe}^2+f_{ce}^2$. Here v_s is the horizontal rocket velocity, h is the source height, t_0 is the time of closest approach of the rocket to the source, and x_0 is the impact parameter, i.e., the distance of closest approach of the rocket to the source magnetic field line.

From the VLF spectrogram (Figure 2a) we scaled the lower boundaries of twelve selected saucer features, illustrated and labeled in Figure 2b. Fitting these points to (1) using a least-squares criterion determines values for t_0, h, and x_0 for each selected saucer feature. Results of these fits are tabulated in the auxiliary materials. The average and range of flight times of closest approach are 382 s and 234–515 s, respectively. The average and range of impact parameters are 90 km and 0–210 km. The average and range of source heights are 2290 km and 1210-3980 km. Similar to the dayside saucers observed with DEMETER [James et al., 2012], these source heights are much farther above the spacecraft than typical for VLF saucers in the auroral zone, as a consequence of their more extended spatial scale.

The large source heights suggest that in the CAPER-2 case, unlike many previous VLF saucer observations, straight-line propagation may not be valid. Therefore, we employed a Python implementation of the 2-D ionospheric whistler mode ray-tracing code based on the Rice [1997] thesis on whistler mode wave propagation adapted by Miroslav Mocak. The code assumes a dipole magnetic field, and impact parameter was set to zero as a limititation of the 2-D code. For the electron density profile, we used the Kletzing and Mozer [1998] model, adjusted to match the density directly measured by CAPER-2 in the topside:

$$n(h) = n_0 e^{-(h-h_0)/r} + n_1 h^b \tag{2}$$

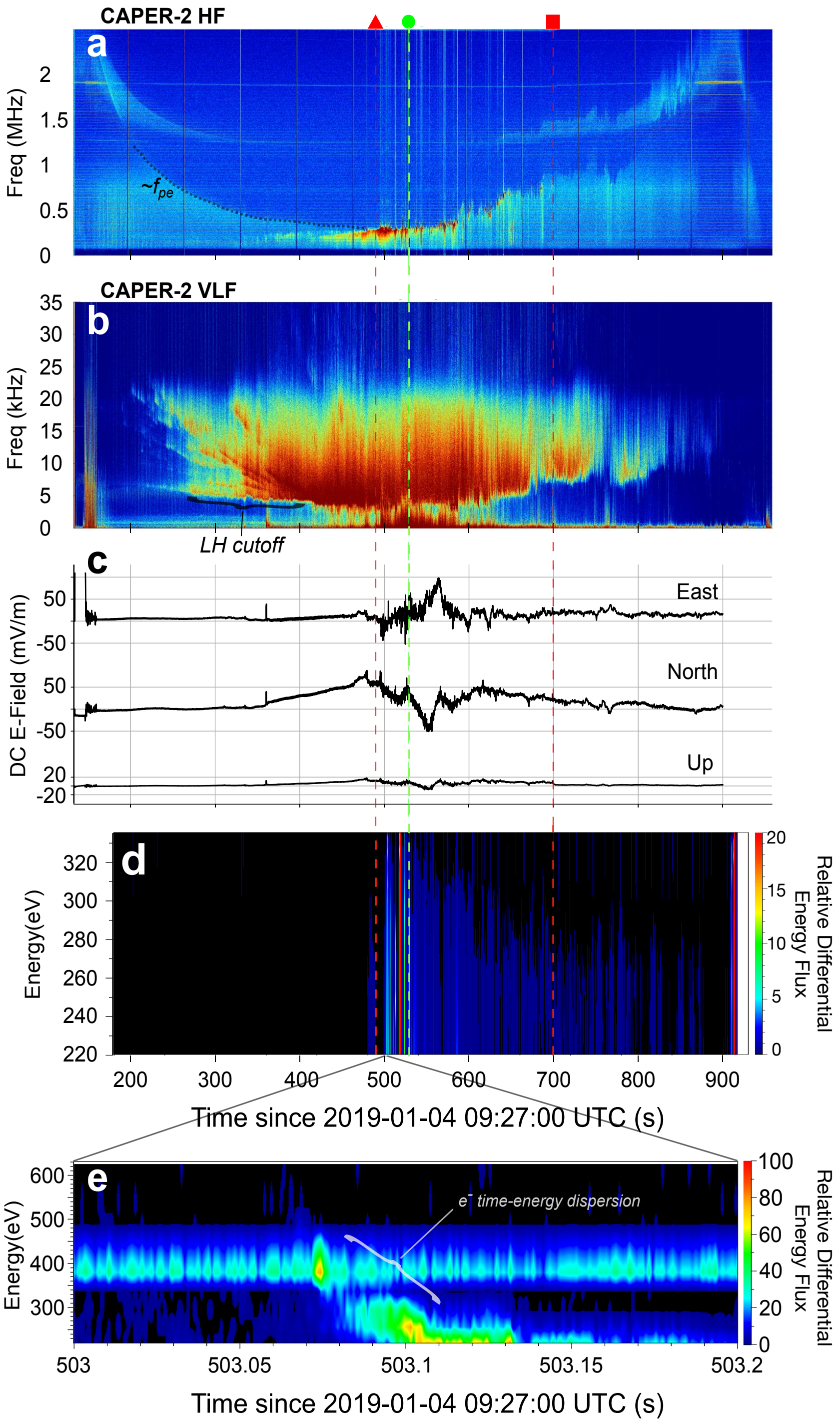

Figure 1. Survey of selected CAPER-2 data. The red triangle and square at top respectively indicate cusp entry (490 s) and exit (700 s). The green circle indicates apogee at 774 km (529s). (a) HF electric field measurements. Intense plasma waves occur during the cusp crossing (∼500–700 s). (b) VLF measurements. Saucer-like features above the lower-hybrid cutoff occur during 200–450 s. (c) DC electric field components. (d) Low-energy parallel electron measurements. An increase in counts indicates soft particle precipitation associated with the cusp. (e) Zoomed view of observed electron time-energy dispersion thought to be associated with Alfvénically accelerated electrons.

where h is the altitude in kilometers from the surface of the Earth, and n_1 and b are parameters from the Kletzing-Mozer model, taken to be $n_1 = 2.68 \times 10^7 cm^{-3}$ and $b = -1.55$ corresponding to the noon sector. Ray-tracing was done for putative sources ranging from 1000 km to 10000 km along the 78° field line, corresponding to the magnetic latitude at which CAPER-2 encountered the cusp; Figure 2d shows example ray paths. A data base was created of ray displacements at 500 km altitude, the average altitude of the CAPER-2 saucer-like features. By matching this data base to the twelve saucer features scaled from Figure 2b, revised source heights were obtained, listed in the auxiliary materials. The average and range of the revised source heights are 2500 km and 1500–4700 km. Saucer features 1-2-6, 3-8-11, and 5-9 appear similar in form (Figure 2b) and not surprisingly correspond to relatively tight ranges of estimated source heights: 2500-2600 km, 1900-2300 km, and 2800-3100 km, respectively.

Whistler mode waves in the ionosphere at frequencies well below f_{pe} or f_{ce} are approximately right-circularly polarized; i.e., the electric field of the wave rotates about the direction of propagation tracing a circle on a hodogram plot of E_x versus E_y in the plane perpendicular to the direction of propagation. CAPER-2 measures the VLF electric field vector in the plane perpendicular to the rocket spin axis which is aligned to within 10° of the magnetic field, which is nearly vertical at high latitudes. If the circularly polarized wave propagates perpendicular to this plane, the instrument would detect the full magnitude of the electric field, yielding a circular pattern when E_x is plotted against E_y. However, if the wave propagates at an angle to the xy-plane the antennas detect an elliptical (pancake-shaped) pattern when E_x is plotted against E_y, which provides direction information about the incoming wave to within a 180-degree ambiguity.

Figures 3a–e show E_x versus E_y hodogram scatterplot for short time intervals during five selected saucer-like signals, labeled 1, 2, 4, 5, and 7 in Figure 2b. The E-field components in these hodograms have been digitally filtered using a bandpass filter with bandwidth 3 kHz and center frequency corresponding to the appropriate saucer-like feature. Figure 3 demonstrates the expected "pancake" pattern. Furthermore, and as expected, the "pancake" features remain fixed in absolute space as the rocket rotates.

Figures 3a–e are snapshots from short intervals when the electric field antennas are oriented geographically north-south and east-west, based on spacecraft attitude which was determined from analysis of on-board gyroscope data combined with sun spikes observed in the DC electric field data. These snapshots show that the last measurements (e.g from the saucer feature labeled 4) suggest east-west propagation, whereas the earliest measurements (e.g from the feature labeled 2) indicate propagation coming from an angle forward (northward) of the east-west line. These measurements are therefore consistent with direction of arrival initially from the northwest and gradually rotating to westward as the rocket approaches the cusp. Figure 3f shows the inferred direction of arrival relative to the east-west line, as a function of time for short intervals within the five saucer-like features. These saucer-like features are the only ones sufficiently separated from other signals and having sufficient signal-to-noise ratio to apply the digital filter and perform the analysis described above.

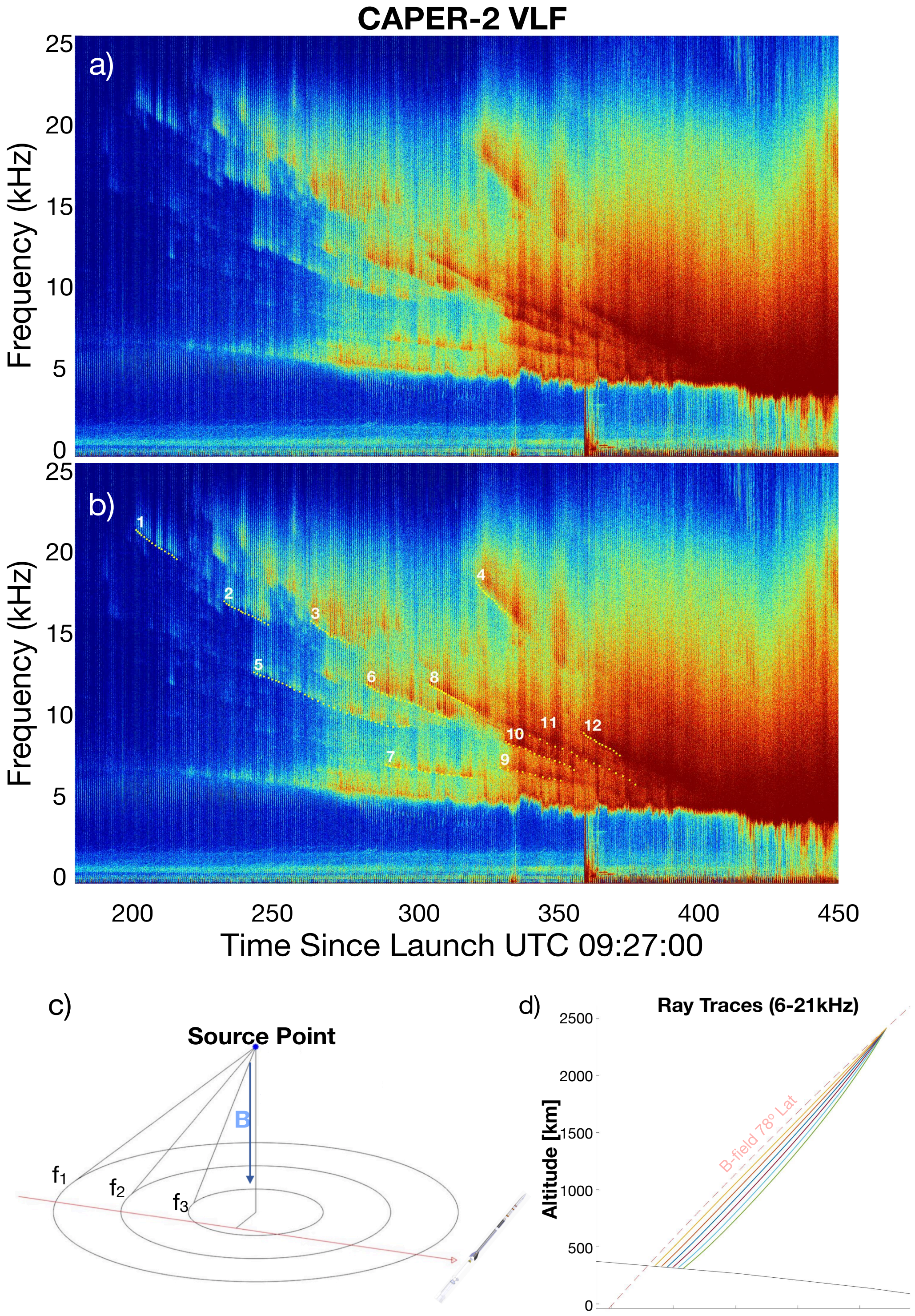

Figure 2. (a) Expanded view of the saucer-like features seen in Figure 1. (b) highlights cut-offs of the 12 selected saucers seen in the top panel.(c) Geometry for generation of saucer feature, assuming straight line propagation [adapted from James, 1976]. (d) ray paths corrected for refraction, calculated with ray tracing code (see text).

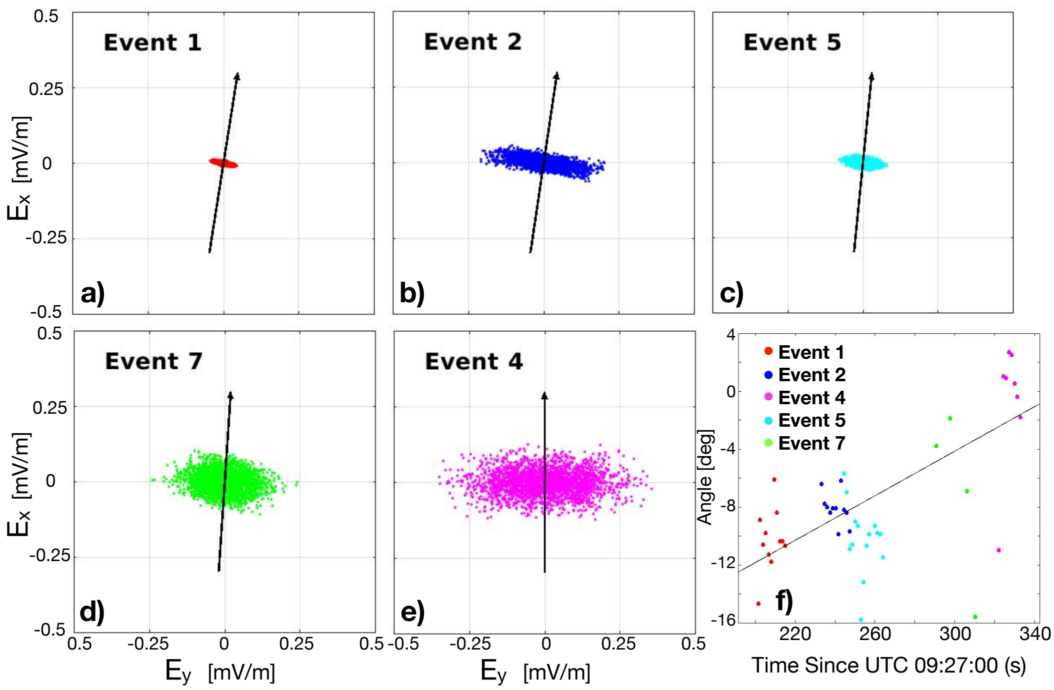

Figure 3. (a-e) Hodogram scatterplots of E_x vs. E_y for five saucer signatures labeled in Figure 2. The pancake-like feature indicates that the wave arrives at an azimuthal angle from source to the rocket, rather than directly downward. (f) shows this angle versus flight time.

3 Discussion

A novel feature of the CAPER-2 experiment was the incorporation of ground based optical and radar data, allowing the large-scale dayside saucers to be placed in the context of these data. Figure 4a shows the CAPER-2 trajectory superposed upon all-sky camera images recorded at Longyearbyen, on Svalbard, in red line (6300 Å, left panel), green line (5577 Å, middle panel), and the ratio of red to green (right panel). Red dominates over green as expected for cusp. While the cusp aurora extend magnetically east and west of the trajectory, the geographic map projection is somewhat misleading as the aurora to the east arises mainly from perspective effect. The map projection of tall rays assuming a fixed emission altitude (250 km for red aurora and 150 km for green aurora) will artificially increase their spatial extent. i.e. the elongated forms to the east of the trajectiory, are likely to be more concentrated closer to the trajectory.

Figure 4b (left panel) shows an image from a hyperspectral camera taken at 0935 UT, corresponding to the time of cusp entry. Figure 4b (right panel) shows the nominal location of the cusp at $\sim$1500km (faded red) and mapped along the magnetic field line to the rocket altitude (solid red), using the Auroral Forecast model [Sigernes, 2016], with the rocket trajectory superimposed. This model is based on the interplanetary magnetic field and solar wind velocity taken from the NOAA-SWPC at the time of the observations. The model agrees with the imager observations, as well as the hyperspectral image. Arrows in Figure 4b are the estimated directions to the saucer sources and impact parameter distances at locations along the trajectory where these could be measured (Figure 4d). The direction of arrival data suggest that the saucer source lies in the cusp aurora on the west side of the trajectory, since the direction shifts from a source northwest to a source west of the trajectory as the rocket approaches the cusp aurora.

As expected, the estimated saucer sources agree more closely with the cusp location (faded red).

Figures 4c show maps of power, Doppler velocity and spectral width of radar backscatter originating from meter-scale irregularities in the cusp, measured with the Hankasalmi SuperDARN radar. These observations are similar to those of Moen et al. [2001]. Gray pixels indicate locations with no backscatter. Radar echoes just to the west of the CAPER-2 trajectory, where the rocket direction of arrival data indicate the source of the saucers, had wide Doppler spreads typical of cusp echoes [Baker et al. 1990]. Figure 4d show profiles of electron temperature and ion outflow measured with the EISCAT radar located just to the west of the CAPER-2 trajectory, showing onset of high electron temperature after 09:30 UT above $\sim$180 km, consistent with the observation of red dominated aurora in the ASI [Vontrat-Reberac et al., 2001; Doe et al., 2001], and suggesting intense precipitation and heating of the electron when CAPER-2 entered the cusp. At the same time ion upflows occur above 250 km. Taken together, the ground based data suggest that the cusp is the source of the large scale saucer features seen by CAPER-2.

A second feature of the CAPER-2 experiment, relative to previous observations of dayside saucers, is complementary high time-resolution electron data. These data show that the cusp is characterized by broadband electrons with energies up to about 400 eV (Figure 1d-e), including dispersed electron bursts. These are characteristic features of Alfvénic acceleration [e.g., Kletzing and Torbert, 1994], and have previously been observed in the cusp [Tanaka et al., 2005]. Figure 1e shows an expanded view of a dispersed feature, having maximum energy of 450 eV and dispersion of about 20 ms. The other observed dispersed electrons had similar characteristics. Estimates of the altitude range over which the electrons are accelerated can be made in two ways. First, the lowest altitude of acceleration should correspond approximately to where the highest observed electron velocities match the Alfvén speed, since the acceleration mechanism boosts the electrons to the Alfvén speed. Using the Alfvén speed model in Chen et al. [2003] (lower trace of their Figure 5), adjusted downward by about 20% to account for about 50% higher F-peak electron density observed by CAPER-2 (9×10^4 cm^{-3} versus 6×10^4 cm^{-3}) yields an estimate of $\sim$ 2000 km. Alternatively one can calculate a distance to the source from the dispersion following Tanaka et al. [2005] which gives 1300 km above the rocket, or about 1900 km. Either of these estimates is comparable to the heights of the saucer sources estimated from the V-shapes. These data suggest that the saucer source may overlap with the region of Alfvénic acceleration, supporting suggestions by James et al. [2012] that Alfvén waves may play a role in dayside saucer generation.

Two other features of the CAPER-2 saucers are worth noting. First, they are asymmetric, occurring on the equatorward side of the cusp but not on the poleward side, whereas examples shown by James et al. [2012] occur on both sides (their Figure 1), although asymmetric saucers have been observed on the nightside [James 1976]. One possible factor in that CAPER-2 is at a lower altitude on the poleward side of the cusp than the quatorward side; however the difference is only 100km which seems inadequate to explain the complete absense of saucers on the polwward side. The difference could also be a temporal effect.

Second, the CAPER-2 saucers are intermittent or "truncated," similar to those observed with DEMETER by James et al. [2012]. In the case of CAPER-2, durations of the pieces of saucers ranged from 5 –50 s. As noted by James et al. [2012], this presents a challenge for theory because the sources must be stationary for these time intervals.

In summary, the CAPER-2 rocket launched into active cusp aurora encountering descending frequency-time signatures in the VLF spectrograms called saucers that are believed to originate from unusually stationary sources in a highly transient medium. These are the first measurements of large-scale saucer features from a sounding rocket on the dayside. Ray tracing and hodogram analysis of the electric field data show the sources

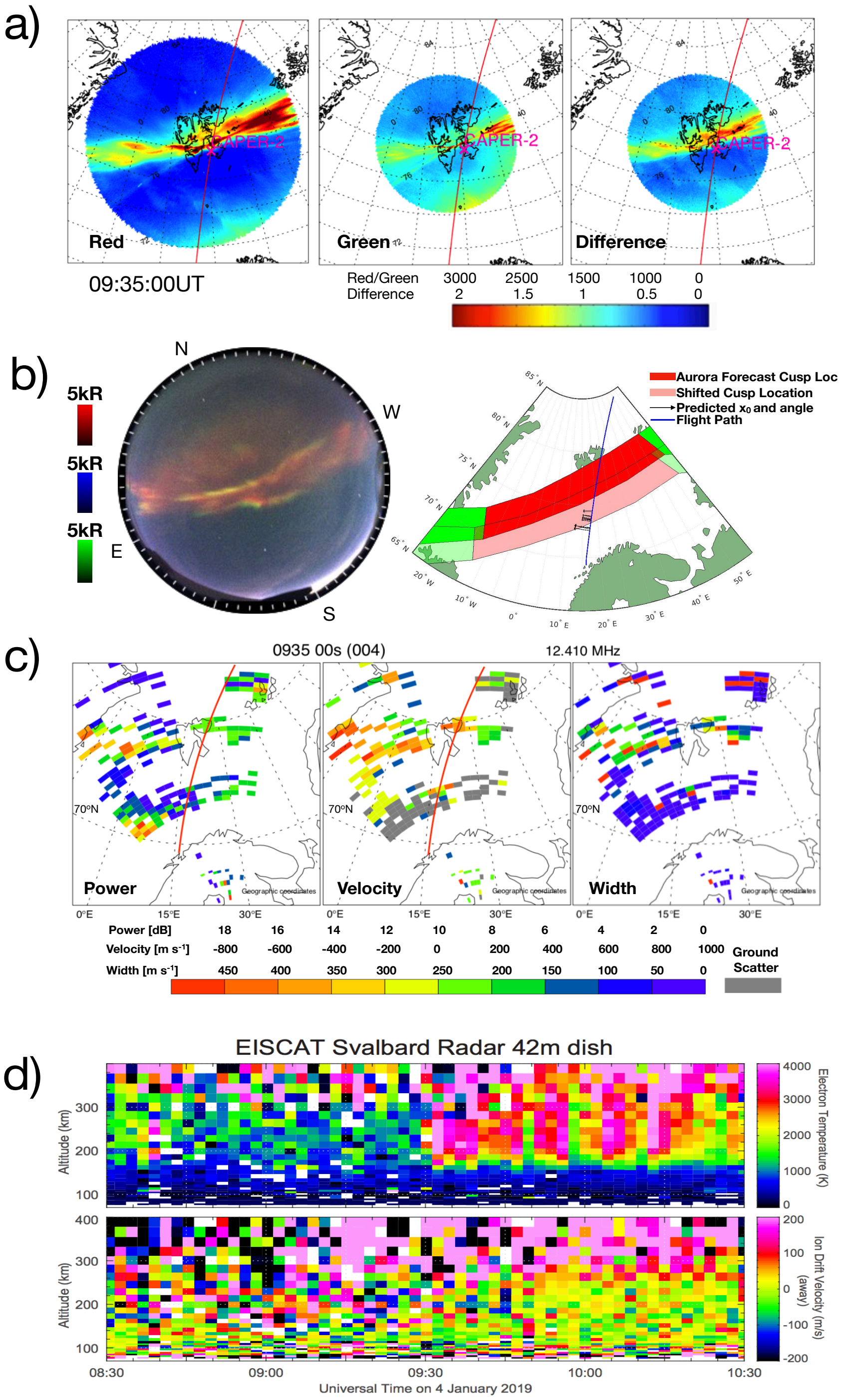

Figure 4. (a) Red (left) and Green (middle), and ratio of red to green (right), line emissions observed by Longyearbyen all sky imager at 480 s with CAPER-2 trajectory superposed. The intense redline over Svalbard is an indication of cusp aurora. (b) Hyperspectral image (left) and predicted cusp location (right) using the Aurora Forecast model. Arrows indicate directions of arrival of the saucer signals along the trajectory inferred from the electric field hodograms. (c) SuperDARN backscatter maps of Doppler power, velocity, and width, with CAPER-2 trajectory superposed. (d) Data from the EISCAT Svalbard Radar, showing onset of high electron temperature and ion upflow after 09:30 UT, suggesting intense precipitation and electron heating as CAPER-2 enters the cusp.

are in the cusp, and particle data suggest Alfvénic auroral acceleration occurs in the same altitude range as the saucer sources.

Acknowledgments

Authors thank: David McGaw, Jeff Dolan, and Espen Trondsen for instrument engineering support; NASA, NSROC, and ASC personnel for supporting launch and payload functions; and KHO, UiO, and UNIS personnel for supporting ground-based data from Svalbard. The Research Council of Norway supported SH, KO, and FS through grant 223252 and JM, AS, and TT through grant 275653. Research at Dartmouth and University of Iowa was supported by NASA grant NNX17AF92G.
EISCAT is an international association supported by research organizations in China (CRIRP), Finland (SA), Japan (NIPR and ISEE), Norway (NFR), Sweden (VR), and the United Kingdom (UKRI):
https://eiscat.se/scientist/data/
Data from the CAPER-2 mission referenced within this article can be found at:
https://phi.physics.uiowa.edu/science/tau/data0/rocket/SCIENCE/CAPERII_Mission/

References

Baker, K., Greenwald, R., Ruohoniemi, J., Dudeney, J., Pinnock, M., Newell, P., . . . Meng, C.-I. (1990). Simultaneous hf-radar and dmsp observations of the cusp. *Geophysical research letters*, *17*(11), 1869–1872.

Chen, F. F., et al. (1984). *Introduction to plasma physics and controlled fusion* (Vol. 1). Springer.

Chen, L.-J., Kletzing, C. A., Hu, S., & Bounds, S. R. (2005). Auroral electron dispersion below inverted-v energies: Resonant deceleration and acceleration by alfvén waves. *Journal of Geophysical Research: Space Physics*, *110*(A10).

Chisham, G., Lester, M., Milan, S., Freeman, M., Bristow, W., Grocott, A., . . . others (2007). A decade of the super dual auroral radar network (superdarn): Scientific achievements, new techniques and future directions. *Surveys in geophysics*, *28*(1), 33–109.

Doe, R., Kelly, J., & Sánchez, E. (2001). Observations of persistent dayside f region electron temperature enhancements associated with soft magnetosheathlike precipitation. *Journal of Geophysical Research: Space Physics*, *106*(A3), 3615–3630.

Ergun, R., Carlson, C., McFadden, J., Strangeway, R., Goldman, M., & Newman, D. (2001). Electron phase-space holes and the vlf saucer source region. *Geophysical research letters*, *28*(19), 3805–3808.

Gurnett, D. A. (1966). A satellite study of vlf hiss. *Journal of geophysical research*, *71*(23), 5599–5615.

Gurnett, D. A., & Frank, L. A. (1972). Vlf hiss and related plasma observations in the polar magnetosphere. *Journal of Geophysical Research*, *77*(1), 172–190.

Horita, R., & James, H. (1982). Source regions deduced from attenuation bands in vlf saucers. *Journal of Geophysical Research: Space Physics*, *87*(A11), 9147–9153.

James, H. (1976). Vlf saucers. *Journal of Geophysical Research*, *81*(4), 501–514.

James, H. G., Parrot, M., & Berthelier, J.-J. (2012). Very-low-frequency saucers observed on demeter. *Journal of Geophysical Research: Space Physics*, *117*(A9).

Kasahara, Y., Yoshida, K.-i., Matsuo, T., Kimura, I., & Mukai, T. (1995). Propagation characteristics of auroral hiss observed by akebono satellite. *Journal of geomagnetism and geoelectricity*, *47*(6), 509–525.

Kletzing, C., & Hu, S. (2001). Alfvén wave generated electron time dispersion. *Geophysical research letters*, *28*(4), 693–696.

Kletzing, C., Mozer, F., & Torbert, R. (1998). Electron temperature and density at high latitude. *Journal of Geophysical Research: Space Physics*, *103* (A7), 14837–14845.

Kletzing, C., & Torbert, R. (1994). Electron time dispersion. *Journal of Geophysical Research: Space Physics*, *99* (A2), 2159–2172.

LaBelle, J., & Treumann, R. A. (2002). Auroral radio emissions, 1. hisses, roars, and bursts. *Space Science Reviews*, *101* (3-4), 295–440.

Lönnqvist, H., André, M., Matson, L., Bahnsen, A., Blomberg, L., & Erlandson, R. (1993). Generation of vlf saucer emissions observed by the viking satellite. *Journal of Geophysical Research: Space Physics*, *98* (A8), 13565–13574.

Moen, J., Carlson, H., Milan, S., Shumilov, N., Lybekk, B., Sandholt, P., & Lester, M. (2001). On the collocation between dayside auroral activity and coherent hf radar backscatter. In *Annales geophysicae* (Vol. 18, pp. 1531–1549).

Mosier, S. R., & Gurnett, D. A. (1969). Vlf measurements of the poynting flux along the geomagnetic field with the injun 5 satellite. *Journal of Geophysical Research*, *74* (24), 5675–5687.

Rice, W. (1997). *A ray tracing study of vlf phenomena* (Unpublished doctoral dissertation). Citeseer.

Sazhin, S., Bullough, K., & Hayakawa, M. (1993). Auroral hiss: A review. *Planetary and space science*, *41* (2), 153–166.

Sigernes, F., Dyrland, M., Brekke, P., Chernouss, S., Lorentzen, D. A., Oksavik, K., & Deehr, C. S. (2011). Two methods to forecast auroral displays. *Journal of Space Weather and Space Climate*, *1* (1), A03.

Smith, R. (1969). Vlf observations of auroral beams as sources of a class of emissions. *Nature*, *224* (5217), 351–352.

Tanaka, H., Saito, Y., Asamura, K., Ishii, S., & Mukai, T. (2005). High time resolution measurement of multiple electron precipitations with energy-time dispersion in high-latitude part of the cusp region. *Journal of Geophysical Research: Space Physics*, *110* (A7).

Temerin, M. (1979). A comment on the source region of vlf saucers. *Journal of Geophysical Research: Space Physics*, *84* (A11), 6691–6693.

Vontrat-Reberac, A., Fontaine, D., Blelly, P.-L., & Galand, M. (2001). Theoretical predictions of the effect of cusp and dayside precipitation on the polar ionosphere. *Journal of Geophysical Research: Space Physics*, *106* (A12), 28857–28865.

Yoshino, T., Ozaki, T., & Fukunishi, H. (1981). Occurrence distributions of vlf hiss and saucer emissions over the southern polar region. *Journal of Geophysical Research: Space Physics*, *86* (A2), 846–852.